Iraqi Journal of Physics, 2026
https://doi.org/10.30723/ijp.v23i2.1410

Vol.24, No.1, PP.142-155
P-ISSN: 2070-4003
E-ISSN: 2664-5548

Investigating the Complex Ring Morphology in UGC 10168: A Photometric and Structural Analysis of a $(R_1R_2')SAB_a(r'l)a$ Galaxy

Zeinab F. Hussein[1*] and Abdullah K. Ahmed[1]
[1]*Department of Astronomy and Space, College of Science, University of Baghdad, Baghdad, Iraq*
[*]Corresponding author: zeinab.hussein@sc.uobaghdad.edu.iq

Abstract
This study provides a comprehensive photometric and structural analysis of the galaxy UGC 10168, which is classified as $(R_1R_2')SAB_a(r'l)a$ in the Comprehensive de Vaucouleurs Revised Hubble-Sandage (CVRHS) system. UGC 10168 is an intermediate barred spiral galaxy with intricate inner and outer ring structures, which presents an intriguing scenario for studying resonant feature dynamics. Surface photometry was used to analyze the luminosity distribution, ellipticity, and position angle profiles along the semi-major axis of the galaxy, utilizing multi-wavelength imaging from the Sloan Digital Sky Survey (SDSS). The classification (R_1R_2') emphasizes the existence of two distinct outer pseudorings that are formed by the winding spiral arms; whereas (r′l) implies an interior, less regular ring that encircles the bar. The galaxy's barred morphology (SAB) and early-type spiral features (Sa) contribute to a complex structural profile, which was analyzed in detail using photometric decomposition techniques. The R_1 and R_2' pseudorings are conceivably associated with the galaxy's bar dynamics and the influence of Lindblad resonances, as our findings disclose notable resonant structures. The colour profiles, calculated from the differences in light intensity between the SDSS filters (g-r, r-i and i-z) were analyzed to understand the gradients in stellar populations and the level of star formation within the rings, bar, and disk. Distinct colour variations between the inner and outer rings indicate differing stellar ages and star-forming areas affected by resonances. This study enhances understanding of ring creation and resonance events in barred spiral galaxies, offering insights into their evolutionary trajectories within galactic dynamics and shape.

Article Info.

Keywords:
Galaxy, CVRHS, UGC 10168, SDSS, Pseudorings.

Article history:
Received:Dec. 18, 2025
Revised: Apr. 18, 2025
Accepted:May, 06, 2025
Published:Mar.01,2026

1. Introduction
Rings are a fascinating component of galactic structure [1]. Barred galaxies are renowned for their ubiquity and the unique ring morphologies they frequently exhibit [2]. Buta and Combes have described the characteristic rings, which consist of nuclear (or circumnuclear), inner, and exterior rings in that order of increasing linear and relative dimensions. The rings are frequently composed of spiral arms that are closely wound (known as "pseudo-rings"), and each form has its own distinctive set of morphological characteristics [3]. Rings remain significant in galactic studies due to their pronounced sensitivity to internal galaxy dynamics and their probable close association with secular evolutionary processes in galactic discs [4].

The outer rings of barred galaxies are about twice as large as the bar. They are believed to be associated with specific orbital resonances in the galactic disk. One of the most common resonances is the outer Lindblad resonance (OLR), which occurs when the pattern speed of the bar matches the difference between the angular rotation speed of the stars and their epicyclic frequency. At the OLR, the stars and gas can be trapped in stable orbits, often forming ring-like structures. In some galaxies, the outer rings may also be linked to a higher-order resonance called the Outer 4:1 Resonance (O4R), where the stars complete four epicyclic oscillations for every full rotation in the frame of the bar. These resonances shape the dynamics and morphology of the outer disk and are key to

understanding ring formation in barred galaxies. [5]. According to de Vaucouleurs's study(1959), outer features have been separated into closed rings (R) and pseudorings (R′) depending on whether the feature is closed or complete [6]. Arms that begin at one end of the bar and terminate at the other end after a 180º bend make up R′ closed rings and R_1' pseudorings [7]. These rings are usually eight-shaped because of a dimpling toward the end of the bar. The two spiral arms that make up R_2 closed rings and R_2' pseudorings begin at one end of the bar and, after a 270° bend, connect approximately perpendicular to the bar's main axis. While R_2' pseudorings are relatively rare, R_2 rings are not identified in the Atlas of Resonance Rings as Known in the S^4G Survey (ARRAKIS). However, the absence of R_2 rings in the atlas may reflect classification uncertainties, since the intrinsic shape of features located at large radii is highly sensitive to the galaxy's orientation and projection effects [8]. Additionally, the Spitzer Survey of Stellar Structure in Galaxies S^4G database has several systematic variety classifications [9]. Inner variants include inner rings (r), inner pseudorings (rs), inner lenses (l), and the pure (s) form. OLR subclass characteristics R_1, R_1', R_2', and R_1R_2' are examples of outer variations, along with no feature for an unclosed spiral, outer pseudorings (R′), outer rings (R), outer ring-lenses (RL), and outer lenses (L) [10].

The morphological categories R_1, R_1', R_2', and R_1R_2' are distinguished from the overall ring population by their unique similarity to model OLR rings [11]. The subclasses are associated with two groups of periodic orbits around the OLR of a bar or oval [12]. Type R_1' (Fig. 1, left) is an external pseudo-ring characterized by an approximately 180° winding of the primary spiral arms from one end of the bar to the other, creating a distinctive figure-eight configuration with 'dimples' that constrict toward the bar axis [13]. This variant may also manifest in a more restricted form, referred to as R_1 [14]. Unlike R_1' outer pseudo-rings, R_2' pseudo-rings are characterized by an approximately 270° winding of the spiral arms in relation to the bar (Fig. 1, right). The salient feature in this case is the duplication of the spiral arms in two opposing quadrants. Although closed R_2 rings are not ruled out, they are harder to identify than R_1 rings due to the lack of clear arm-doubling. Interesting, some galaxies show a hybrid form that combines elements of both types, classified as R_1R_2', $R_1'R_2'$, or R_1R_2. In such hybrid systems, the morphology reveals the presence of both families of OLR periodic orbits (Fig. 1, middle) [15].

Buta (1995) determined via a comprehensive investigation of the Catalogue of Southern Ringed Galaxies (CSRG) that R_1 and R_1' rings are more prevalent than R_2' rings, with a relative percentage of 0.64:0.36. In the GZ2 repertoire, R_1' and R_2' were nearly equally represented, whereas R_1 and R_2' were less prevalent than either [16]. Table 1 gives explanations of CVRHS symbols.

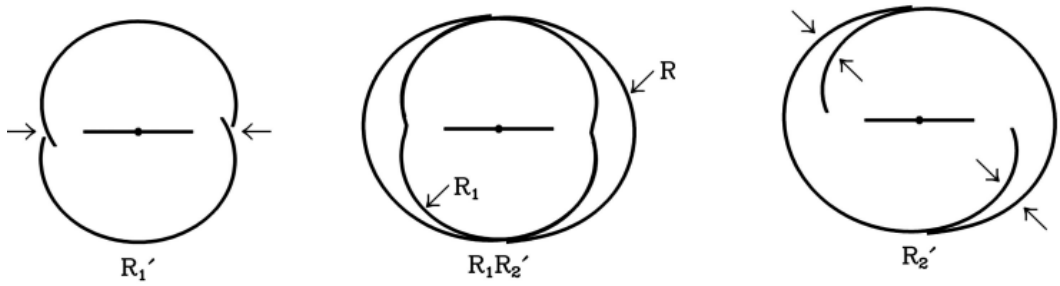

Figure 1: Diagrams showing the pseudo-ring and outer resonant ring morphologies [15].

Table 1: CVRHS Symbols Explanation [17].

Outer variety	feature of galaxy morphology that identifies a big ring or pattern resembling a ring in a galaxy's outer regions
R_1'	An outer pseudoring made from arms that wind about 180° with respect to the bar ends; an OLR subclass
R_2'	An outer pseudoring made from arms that wind about 270° with respect to the bar ends; an OLR subclass
R_1R_2'	A combined outer ring-pseudoring pattern where the arms forming the R_2' ring break from an R1 ring; an OLR subclass
R_{12}'	An unusual version of (R_1R_2') where only half of each feature is seen
R_1	A closed outer ring showing a shape resembling a broad figure 8; a subtly dimpled oval ring, recognized as an OLR subclass

Barred galaxies like UGC 10168, characterized by distinct ring structures, are crucial for investigating resonance dynamics, since these rings delineate gas distribution, star formation areas, and resonance phenomena [18]. The colour distribution across the galaxy, particularly in rings and bars, offers significant insights about stellar age gradients and star formation, therefore clarifying the evolutionary processes that have shaped the galaxy's appearance [19]. Photometric study of UGC 10168, namely in the g-r and r-i color indices, enables the examination of stellar age gradients and star formation activity across its unique physical characteristics. This research employs multi-wavelength imaging data from the Sloan Digital Sky Survey (SDSS) to conduct an extensive photometric and structural examination of UGC 10168 [20]. The galaxy's light distribution, color gradients, and structural characteristics were analyzed along the semi-major axis by surface photometry and photodecomposition. The aim of this study is to enhance our comprehension of the mechanisms that govern ring development and resonance in barred spiral galaxies by analyzing the inner and outer rings, as well as the intermediate bar. The findings have significant implications for examining galactic morphology and the influence of resonance on the formation of galaxy structures. The basic details of UGC 10168 are shown in Table 2.

Table2: The UGC 10168 Galaxy's Fundamental Information.

UGC 10168	
Morphology	(R)SAB0/a*
CVRHS Classification	$(R_1R_2')SAB_a(r'l)a$ ****
RA (deg)	240.881765*
DEC (deg)	49.338157*
Redshift	0.02007*
Semi major axis (kpc)	49.2 *
Inclination (deg)	40.2 **
Position Angle (deg)	172.4 **
Apparent magnitude in B-band (mag)	14.02 **
SDSS Name	SDSS J160331.62+492017.3***
Observation Date (M/D/Y)	04/05/2000 ***
File Name	fpC-001345-x2-0580 ***

* NED, ** HyperLEDA, ***SDSS, **** (CVRHS) Classification, X is the filter name.

2. Data and Observational Sources

The SDSS provides the optical data and images for UGC 10168 [21]. The images are available in FITs (Flexible Image Transport System) format, which is a standard digital file format in astronomy used to store, transmit, and process scientific images and data. More specifically, structural and color analyses were performed using imaging data in several optical bands: g (green), r (red), i (near infrared), and z (infrared). As a large-scale astronomical survey, SDSS provides high-quality imaging and spectroscopic data across wide areas of the sky, making it a valuable resource for studying galaxy morphology and stellar populations. Standard photometric analysis and surface brightness decomposition methods were then applied to examine the structural properties of the galaxy and its ring [22, 23]. The galaxy's CVRHS classification is (R_1R_2') SAB_a(r'l)a, as shown in Fig. 2.

The central bar in UGC 10168 exhibits prominent ansae structures, which appear as symmetric brightness enhancements at both ends of the bar, often aligned with its major axis. These features are commonly observed in early-type barred galaxies and have been discussed in several recent studies. According to Martinez-Valpuesta et al. (2007), approximately 40% of early-type barred galaxies show evidence of ansae, suggesting a link with advanced dynamical evolution of the bar [24]. Furthermore, Athanassoula (2002) demonstrated that ansae formation is connected to long-term dynamical interactions between the bar and the dark matter hallo, where angular momentum transfer from the bar to the halo leads to bar growth and the development of terminal enhancement [25].

In this study, the presence of ansae was identified through surface brightness profile and isophotal contour maps, which clearly revealed elongated and bright ends separating the bar from the inner ring structure. This supports the CVRHS classification of the galaxy as (R_1R_2')SAB_a(r'l)a.

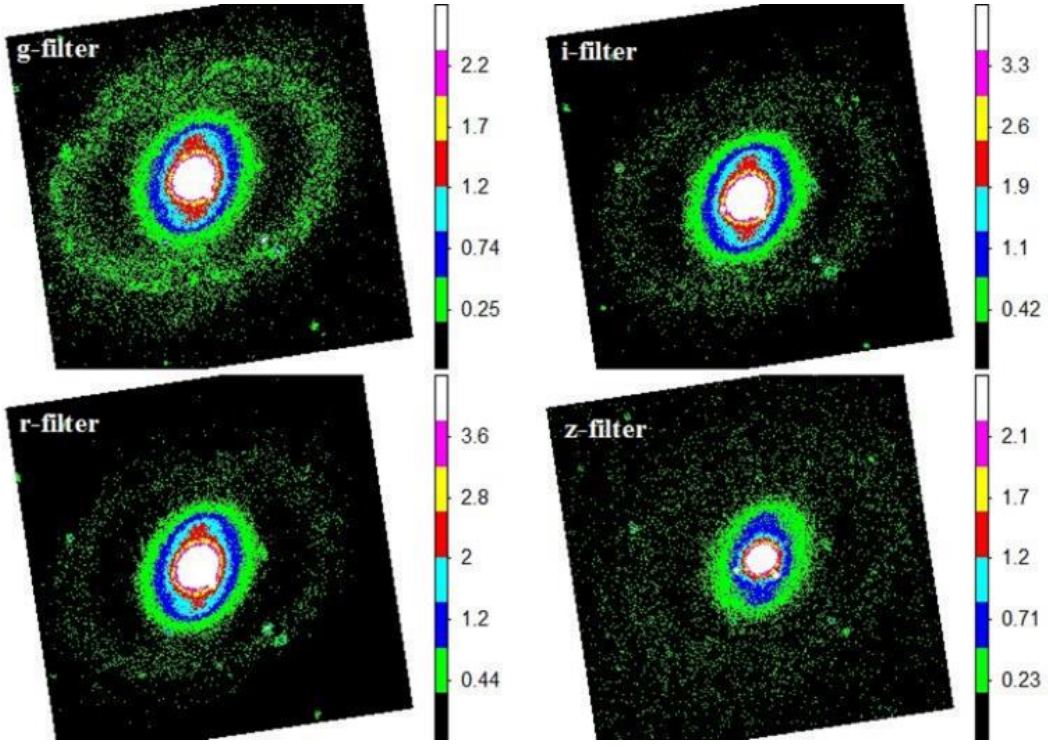

Figure 2: From left to right, fuzzy color photos of UGC 10168 using griz-filters. East is left, and north is up.

3. Data Reduction

The observation data of the galaxy image frames was reduced using the following methods:

Function: imcopy: the imcopy function from IRAF (Image Redaction and Analysis Facility) was used to extract the area surrounding the target galaxy from the original image frames. IRAF is a widely used software system in astronomy for the processing and analysis of astronomical data. By using this function, the galaxy was isolated within a smaller and more manageable rectangular region of the image.

Function: imexam and imarith: imexam was used to measure the intensity of the sky backdrop, and then imarith was used to remove it from each galaxy frame.

Pixel Value Conversion to Arcsec^2: The pixel scale was converted to arcsec^2 units depending on the picture resolution. For pixel scale, the SDSS picture information (usually 0.396 arcsec/pixel for SDSS) was used.

Function: imarith: each galaxy frame was divided by the exposure duration to standardize the intensity to a one-second exposure.

Convert Flux to Magnitude Units: Eq. (1) was used to convert each frame's intensity flux value (I) into magnitudes [26].

$$m = 2.5 \log \left(I \times 10^{(z_p + k_a + \text{airmass})}\right) \quad (1)$$

where the airmass represents the optical path length that light from a celestial object travels through Earth's atmosphere, expressed relative to the path length at the zenith (where air mass equals 1) [27, 28]. Atmospheric extinction is denoted by (K_a) and the zero-point magnitude by (z_p), as shown in Table 3.

Table 3: The zero point magnitude (z_p), an atmospheric extinction (k_a), and an airmass for UGC 10168 galaxy [29].

Galaxy	filters	air mass	Zero point (z_p)	Atmospheric Extinction (K_a)
UGC 10168	g	1.1022	24.485	0.1723
	r	1.1082	24.088	0.10559
	i	1.10667	23.52	0.06431
	z	1.1367	21.989	0.0624

4. Results and Discussion

4.1. UGC 10168 Morphologies and Contour Maps

The isophotal contour maps of the UGC 10168 galaxy reveal its surface brightness distribution in different filters, providing insights into its structure and morphology. Key features include a well-defined bulge in the central region, a bar structure, an inner pseudoring-lens (r'l), and outer rings (R_1 and R_2'). The bar's presence redistributes gas and stars, fueling the formation of the inner and outer rings. The inner pseudoring-lens structure may be located near resonant, such as the O4R or ILR, where gas and stars are trapped in elliptical orbits. The outer rings are products of OLRs, where spiral arms intersect and form pseudorings [30]. The well-defined rings and dominant bulge suggest UGC 10168 is in an advanced stage of secular evolution, with the bar and rings contributing to its current morphology. Fig. 3 illustrates Isophotal Contour Maps of the UGC 10168 galaxy in the gri and z- filter. Levels of surface luminance are specified in Table 4.

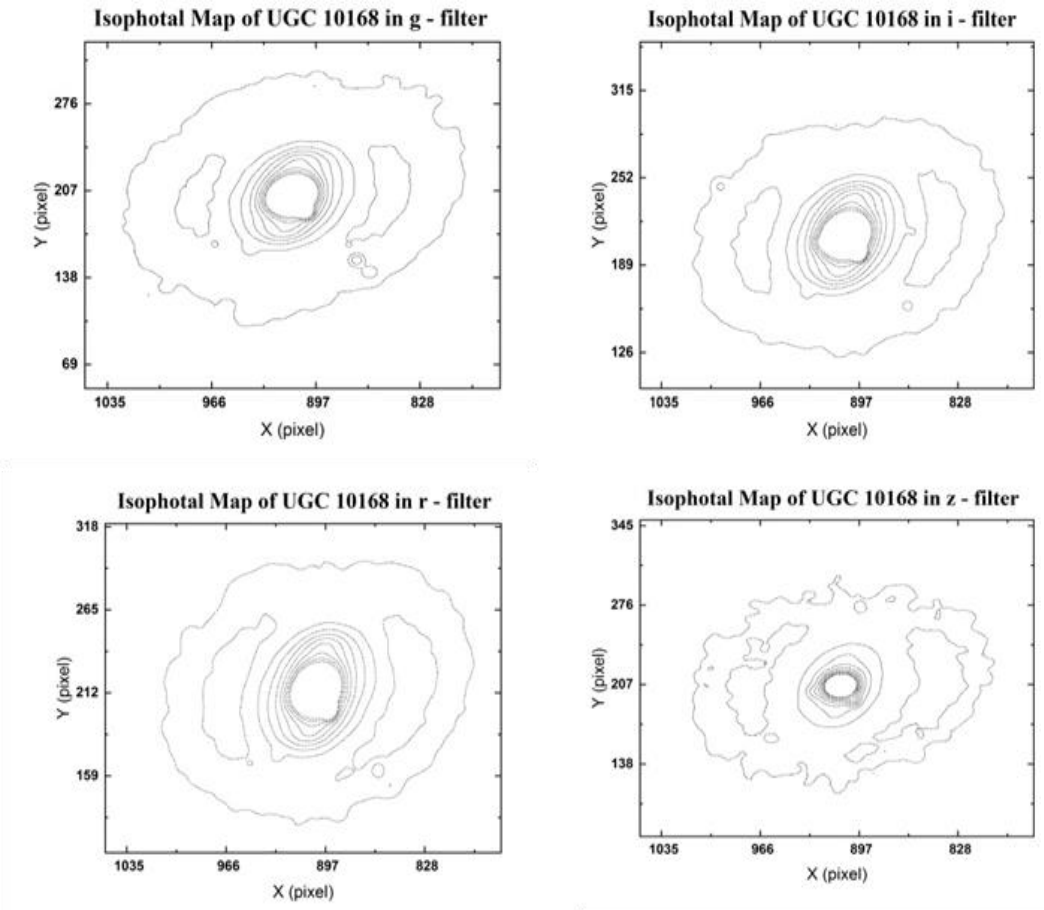

Figure 3: Isophotal Contour Maps of UGC 10168 galaxy in gri and z- filter, North is up and East is left.

Table 4: The surface brightness levels of the griz outer isophotes of the UGC 10168 galaxy.

Galaxy	Filter	Surface brightness of Outer isophot (mag/arc sec ^{2})	Apparent magnitude of Outer isophot (mag)	Step
UGC 10168	g	21.530	23.542	0.247
	r	20.764	22.77	0.36
	i	20.33	22.34	0.337
	z	18.87	20.88	0.288

4.2. Structural Parameters

The distributions of magnitude, Fourier coefficient (B4), position angle (PA), and ellipticity are presented in Fig. 4, arranged in a clockwise direction starting from the top left. The overall distribution pattern of each parameter is nearly the same across all filters.

In Fig. 4 (top left), the radial surface brightness profiles of UGC 10168 are shown for the g, r, i, and z filters. The profiles followed a general exponential decline, indicating a disk-dominated structure. Between radii of approximately 4 to 6 arcsec, a noticeable plateau or excess brightness was observed, especially in g and r bands. This plateau is likely associated with the inner pseudoring-lens structure (r'l), reflecting a stellar accumulation in resonant orbits. The inner slope of the profile was relatively shallow, influenced by the central bulge and bar component. At radii ~ 10 arcsec, the profile steepened significantly, marking the transition to the outer disk and component pseudoring regions (R_1 and R_2'). These features are consistent with a multicomponent

galaxy undergoing bar-driven secular evolution, as described in recent photometric studies [31].

In Fig. 4 (top right), the observed variations in the B_4 Fourier coefficient across the semi-major axis provided insight into the morphological evolution of the UGC 10168. Positive B_4 values in the inner regions indicate disky isophotes, likely shaped by the bar's gravitational potential and the resulting orbital families near the inner Lindblad resonance. In contrast, near-zero or negative B_4 values at intermediate radii may correspond to the ring structures, where stellar orbits were more circular or boxy due to resonance trapping.

In Fig. 4 (bottom left), the Position Angle (PA), which indicates the orientation of the galaxy's structures, started steady but then showed a brief variation. This might suggest that the inner bar or ring is slightly misaligned with the surrounding structures. A sudden jump to 179.6° marks the transition from the inner bar region to the outer disk or ring components. At larger semi-major axis values, the PA changes gradually but stays within a range of 170° to 175°, likely influenced by the spiral arms or inner pseudorings. Between 4 and 8 arcsec, the PA shifted more noticeably, dropping to values between 110° and 150°. This could reflect twisting or warping in the outer parts of the bar or the start of the spiral arms. Beyond this, the PA stabilized somewhat, settling between 109° and 128°, though small oscillations persisted. This apparent misalignment between inner and outer regions may be attributed to the intrinsic elongation of R_1 rings, which are typically aligned perpendicular to the bar, as was shown in previous studies by Schwarz (1984) [32], Kormendy (1979) [33], and Buta (1995) [16].

In Fig. 4 (bottom right), the ellipticity of the galaxy started high, which suggests an elongated core structure. It then gradually decreased, possibly because the inner bar or ring changed into a more circular shape. After that, the ellipticity increased slightly, indicating a shift from the central bar to a more rounded inner region or a ring-like structure. Between 3 and 6 arcsec, the ellipticity rose steadily, likely due to the presence of outer pseudorings or the influence of spiral arms. From 6 to 10 arcsec, it showed a noticeable increase, reaching values between 0.28 and 0.35 around 8 arcsec. This marks the transition to the outer spiral arms or outer pseudoring. The highest ellipticity corresponds to the area of greatest elongation, which may occur as the pseudoring structure becomes more diffuse at larger distances. Beyond this point, the ellipticity stabilized at around 0.25, indicating the dominance of the galaxy's main disk, with no significant additional changes observed at larger semi-major axis values.

4.3. Surface Brightness Profiles Decomposition

De Vaucouleur's law $r^{1/4}$, which simulates the circular decrease in surface brightness with increasing radial distance from the galaxy center, is often used to characterize the bulge of galaxy. Eq. (2) expresses this law [34, 35]

$$\mu_{bulge}(r) = \mu_e + 8.3268 \left[\left(\frac{r}{r_e}\right)^{1/4} - 1\right] \quad (2)$$

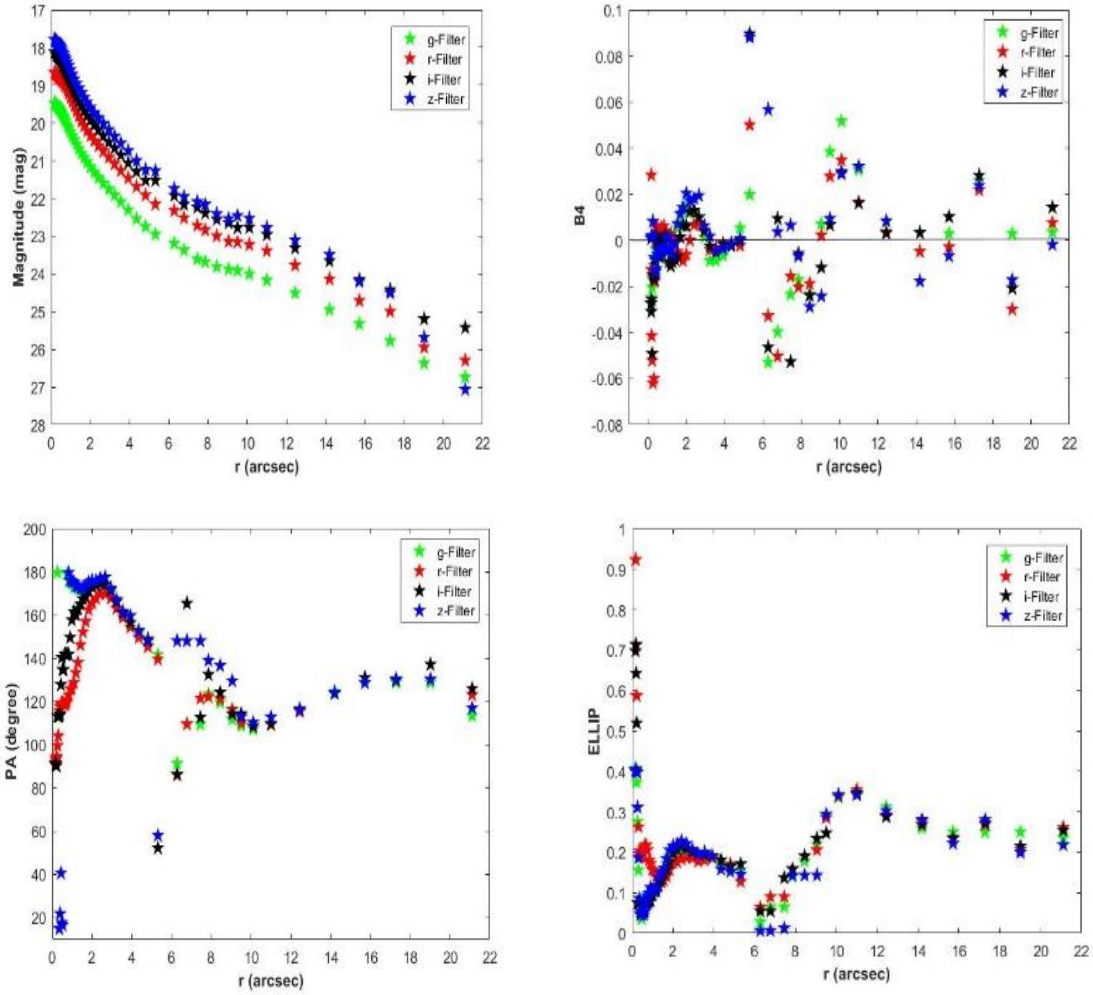

Figure 4: The magnitude (top left), Fourier coefficient (B4) (top right), position angle (PA) (lower left), and ellipticity (lower right) as function of semi major axis of the UGC 10168 galaxy.

Eq. (3) shows that the disk's brightness profile is exponential [36, 37]

$$\mu_{disk}(r) = \mu_0 + 1.09 \left(\frac{r}{r_0}\right) \quad (3)$$

At effective radius r_e, when half of the light is radiated inside r_e, the surface brightness is denoted by μ_e. The symbols μ_e and r_0 represent the center surface brightness and disk scale length, respectively. It should be mentioned that μ_0 is not directly measured because it only represents the brightness of the disk component and not the galaxy's center surface.

The relationship between the galaxy radius (r) in the griz filters and the surface brightness fit of the bulge and disk structure of the UGC 10168 is seen in Fig. 5. Table 5 presents the UGC 10168's decomposition parameters. 10168's The UGC surface brightness profiles indicate that these galaxies' outer disks were type I Freeman [38].

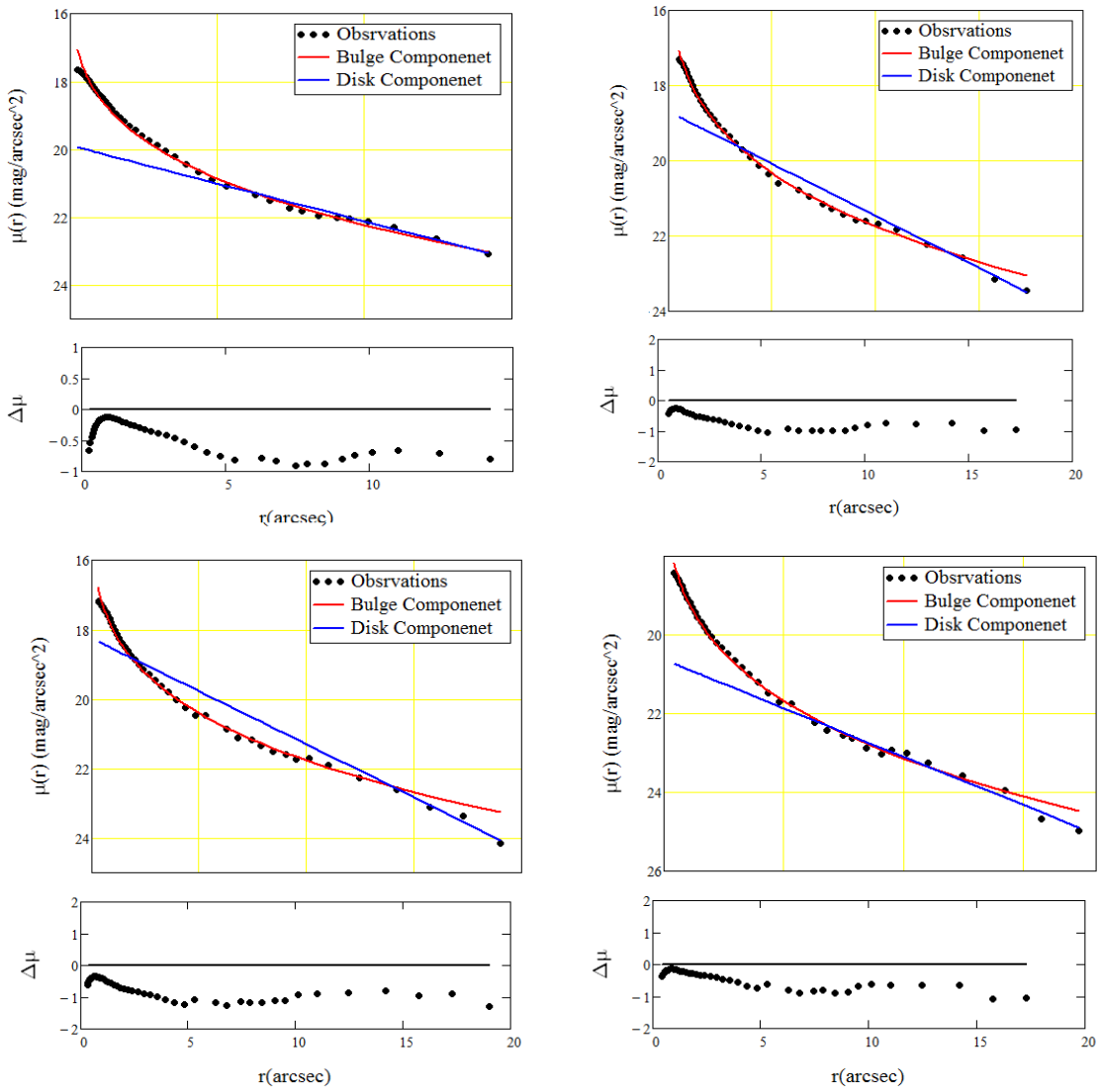

Figure 5: Decomposition of griz-band surface brightness profiles between the observed data for the UGC 10168 galaxy and the (Bulge+Disk) model. From top left to right, griz-filters.

Table 5: UGC 10168's Decomposition Parameters.

		Bulge				Disk					
	Filter	**Range (arcsec)**	**μ_e (mag/arcsec^2)**	**r_e (arcsec)**	**Standard error**	**μ_o (mag/arcsec^2)**	**r_o (arcsec)**	**Standard error**	**Apparent magnitude (mag)**	**Apparent magnitude (mag) from SDSS**	**Bulge to Disk ratio**
UGC 10168	g	0.39-9.04	21.972	8.801	0.041	19.89	4.86	0.015	13.86	14.06	0.91
	r	0.57-12.43	21.158	7.612	0.026	18.69	3.91	0.049	13.36	13.17	0.74
	i	0.34-12.43	21.533	8.925	0.038	18.25	3.55	0.052	13.39	12.73	0.58
	z	0.47-7.85	22.315	6.85	0.031	20.63	4.39	0.06	14.74	12.45	0.97

A quantitative uncertainty analysis was conducted for the photometric decomposition parameters listed in Table 5. The standard errors associated with the effective surface brightness (μ_e), effective radius (r_e), central surface brightness (μ_0), and scale length (r_0) were derived from the fitting procedure using a least-squares minimization method. These errors reflect the confidence intervals of the fitted parameters. They indicate the model's sensitivity to the observed surface brightness distribution.

Statistical error propagation was applied to validate the reliability of the decomposition, particularly for the derived Bulge-to-Disk ratio (B/D), using the uncertainties of individual parameters. In addition, the stability of the fitted values was confirmed by repeating the decomposition across different radial ranges and with perturbed profiles to simulate observational noise. The consistent results supported the robustness of the fitting procedure and indicated that the reported values fall within acceptable statistical limits.

4.4. Color Index

The colour profiles, (g-r, r-i, and i-z) which represent differences in brightness between SDSS filter, are shown along the semi-major axis in Fig. 6.

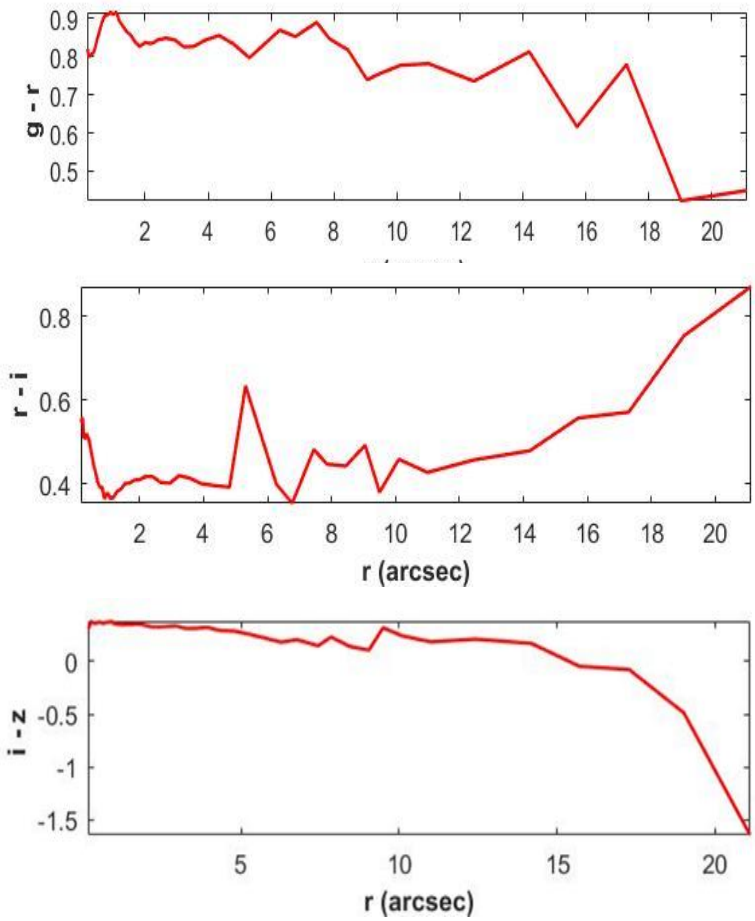

Figure 6: g-r, r-i, and i-z color profiles of UGC 10168.

The $(g-r)$ values in the galaxy fluctuated from 0.76 to 0.83, possibly due to inner pseudoring or bar-driven star formation. From 3 to 6 arcsec, the values stabilized, possibly in outer pseudoring regions. From 6 to ~15 arcsec, the values became more variable, possibly indicating spiral arms. The values decreased significantly in the outer regions, the values decreased significantly, indicating a shift to bluer colors.

The (r - i) values in a galaxy's core ranged from 0.58 to 0.49, indicating a redder core with older, more metal-rich stars. From 1 to 3 arcsec, values decreased to 0.40-3.38, suggesting a well-established population of intermediate-age stars and minimal dust. From 3 to 6 arcsec, values fluctuated between 0.38 and 0.41, suggesting spiral arm structures or outer pseudoring with a mix of younger and intermediate-age stars. From 6 to 15 arcsec, values varied significantly, ranging from 0.35 to 0.49, with some outliers. In the outer regions, values rose sharply, reaching 0.87 at the farthest semi-major axis, possibly due to dust or extended old stellar populations in the outer disk or halo.

The (i−z) values in a star's core ranged from 0.35 to 0.33, suggesting a red core with an older, possibly metal-rich stellar population. From 1 to 3 arcsec, the values remained stable, indicating a homogeneous stellar population. From 3 to 6 arcsec, the values decreased, suggesting younger stellar populations or lower metallicity stars dominate. Beyond 6 arcsec, i−z values showed significant fluctuations, suggesting active star formation in spiral arms. In regions over 15 arcsec, i−z values dropped dramatically, reaching very low or negative values, possibly indicating significant young star populations.

In summary, the galaxy exhibited a redder center region dominated by older stars, gradually transitioning to bluer outer populated by younger stars, reflecting its complex structure of rings, spiral arms, and active star-forming regions.

4.5. Comparative Analysis with Similar Galaxy

To place the UGC 10168 galaxy in a broader morphological and photometric context, its structural and color properties were compared with a sample of similar barred spiral galaxies classified as (R_1R_2') or $SAB_a(r'l)a$. Table 6 summarizes the main similarities and differences in terms of ring morphology, bar dynamics, and color gradients. UGC 10168 exhibits a well-defined inner ring and an outer pseudoring consistent with the R_2' type. The bar is moderately developed, and the g–r color gradient shows a smooth outward reddening. This behavior is comparable to the NGC 3081 galaxy, which also shows clear resonance ring structures.

Such comparison highlights the diversity within the (R_1R_2') and $SAB_a(r'l)a$ classes and emphasizes the role of bar strength and secular evolution in shaping the morphology and stellar population gradients in ringed galaxies.

This broader context strengthens the interpretation of UGC 10168 as a transitional case with intermediate bar dynamics and color structure, potentially influenced by internal resonance-driven processes rather than external interactions.

Table 6: Comparing Galaxy UGC 10168 with a Similar Galaxy.

Galaxy	Morphological Type	Ring Structures	Bar Characteristics	Color Gradients	Reference
UGC 10168	$(R_1R_2')SAB_a(r'l)a$	Outer R_1 and R_2'; inner r′l structure	Weak bar, intermediate	Smooth, outward reddening	This study
NGC 3081	$(R_1R_2')SAB(r)a$	Prominent R_1 and R_2'	Weak bar	g–r increases with radius	R. J. Buta (1990) [39], G. G. Byrd et al. (2006) [40]

5. Emission Line Analysis of UGC 10168

Based on the spectrum of UGC 10168, the [OII] (λ=3727) emission line was notably absent, while other prominent lines were clearly detected, as shown in Fig. 7. The spectrum is dominated by Hα, [NII], and [OIII] emission lines, which indicate the

presence of active star-forming regions and metal-rich interstellar medium. Hβ and [SII] lines were also present, though less prominent, offering additional insight into the physical conditions of the ionized gas. The absence of the [OII] line may suggest either low ionization star formation activity or significant dust attenuation at shorter wavelengths.

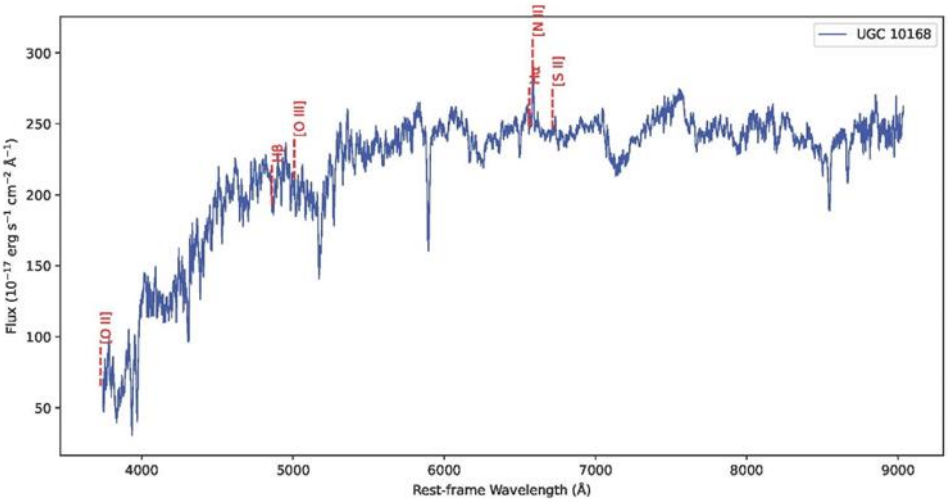

Figure 7: The UGC 10168 galaxy's spectra.

The spectroscopic observation was conducted at an airmass of 1.0923, as reported in the SDSS DR16 database (Plate 622, MJD 52054, and Fiber 356). This moderately low airmass suggests limited atmospheric extinction, supporting the reliability of the measured emission line fluxes and their use in evaluating star formation and metallicity.

6. Conclusions

UGC 10168, a galaxy with mixed morphological features, is classified as $((R_1R_2')SAB_a(r'l)a)$ within the CVRHS system. Its complex structure includes inner and outer resonance rings, a weak bar, and a transitional morphology between elliptical and late-type spiral galaxies. Photometric profiles revealed a brightness profile that decreased outward from the core, suggesting a highly structured galactic environment. The color profile analysis may indicate variations in the stellar population, with a redder core indicating older stars and bluer outer regions indicating ongoing star formation. The complex ring structures and bar dynamics align with the hypothesis that ringed and barred galaxies form through resonances induced by interactions or internal dynamical processes. The dual-ring structure suggests that UGC 10168 may have undergone past gravitational interactions or instabilities, contributing to its present morphology. Based on the analysis and processing findings, it was discovered that the brightness profile of UGC 10168's outer disks is type I Freeman,

Acknowledgment

We thank the Sloan Digital Sky Survey for providing the observational data used in this research. This study used the NASA/IPAC Extragalactic Database (NED), managed by the Jet Propulsion Laboratory at the California Institute of Technology, under contract to the National Aeronautics and Space Administration (NASA). In addition, we used the Bibliographic Services of the NASA Astrophysics Data System. We also thank the use of the Hyper-LEDA database (http://leda.univ-lyon1.fr).

Conflict of Interest

The author(s) declare that there is no conflict of interest.

References

1. B. M. Pakdil, M. Mangedarage, M. S. Seigar, and P. Treuthardt, Monthly Notices of the Royal Astronomical Society, **466**(1), 355 (2017). https://doi.org/10.1093/mnras/stw3107.
2. J. Fernandez, S. Alonso, V. Mesa, F. Duplancic, and G. Coldwell, Astronomy & Astrophysics, **653**, A71 (2021). https://doi.org/10.1051/0004-6361/202141208.
3. D. Krishnarao, Z. J. Pace, E. D'Onghia, J. A. L. Aguerri, R. L. McClure, T. Peterken, J. G. Fernández-Trincado, M. Merrifield, K. L. Masters, and L. Garma-Oehmichen, The Astrophysical Journal, **929**, 112 (2022). https://doi.org/10.3847/1538-4357/ac5d55.
4. G. Blázquez-Calero, E. Florido, I. Pérez, A. Zurita, R. J. Grand, F. Fragkoudi, F. A. Gómez, F. Marinacci, and R. Pakmor, Monthly Notices of the Royal Astronomical Society, **491**, 1800 (2020). https://doi.org/10.1093/mnras/stz3125.
5. J. Fernandez, S. Alonso, V. Mesa, and F. Duplancic, Astronomy & Astrophysics, **683**, A32 (2024).https://doi.org/10.1051/0004-6361/202245215.
6. A. B. Romeo, O. Agertz, and F. Renaud, Monthly Notices of the Royal Astronomical Society, **518**, 1002 (2023). https://doi.org/10.1093/mnras/stac3074.
7. M. Padave, S. Borthakur, H. B. Gim, D. Thilker, R. A. Jansen, J. Monkiewicz, R. C. Kennicutt, G. Kauffmann, A. J. Fox, and E. Momjian, The Astrophysical Journal, **960**, 24 (2023). https://doi.org/10.3847/1538-4357/ad029b.
8. I. Breda and P. Papaderos, Astronomy & Astrophysics, **669**, A70 (2023). https://doi.org/10.1051/0004-6361/202245095.
9. Y. Rashed, M. Al Najm, and H. Al Dahlaki, Baghdad Science Journal, **16**, 230 (2019). http://dx.doi.org/10.21123/bsj.2019.16.1(Suppl.).0230.
10. S. A. A. Albakri, M. N. A. Hussien, and H. Herdan. in *IOP Conference Series: Materials Science and Engineering*. IOP Publishing, **757**, 012043 (2020).https://doi.org/10.1088/1757-899X/757/1/012043.
11. L. Scaloni, G. Rodighiero, A. Enia, C. Gruppioni, F. Annibali, L. Bisigello, P. Cassata, E. M. Corsini, V. Casasola, and C. M. Lofaro, Astronomy & Astrophysics, **687**, A255 (2024). https://doi.org/10.1051/0004-6361/202449894.
12. S. J. Kruk, C. J. Lintott, S. P. Bamford, K. L. Masters, B. D. Simmons, B. Häußler, C. N. Cardamone, R. E. Hart, L. Kelvin, and K. Schawinski, Monthly Notices of the Royal Astronomical Society, **473**, 4731 (2018). https://doi.org/10.1093/mnras/stx2605.
13. J. A. Sellwood and K. L. Masters, Annual Review of Astronomy and Astrophysics, **60**, 73 (2022). https://doi.org/10.1146/annurev-astro-052920-104505.
14. R. J. Buta, Monthly Notices of the Royal Astronomical Society, **488**, 590 (2019). https://doi.org/10.1093/mnras/stz1693.
15. R. J. Buta, Monthly Notices of the Royal Astronomical Society, **470**, 3819 (2017). https://doi.org/10.1093/mnras/stx1392.
16. R. J. Buta, Astrophysical Journal Supplement Series, **96**, 39 (1995).
17. R. J. Buta, K. Sheth, E. Athanassoula, A. Bosma, J. H. Knapen, E. Laurikainen, H. Salo, D. Elmegreen, L. C. Ho, and D. Zaritsky, The Astrophysical Journal Supplement Series, **217**, 32 (2015). https://doi.org/10.1088/0067-0049/217/2/32.
18. K. W. Willett, M. A. Galloway, S. P. Bamford, C. J. Lintott, K. L. Masters, C. Scarlata, B. D. Simmons, M. Beck, C. N. Cardamone, and E. Cheung, Monthly Notices of the Royal Astronomical Society, **464**, 4176 (2016). https://doi.org/10.1093/mnras/stw2568.
19. L. Gutiérrez, P. Erwin, R. Aladro, and J. E. Beckman, The Astronomical Journal, **142**, 145 (2011). https://doi.org/10.1088/0004-6256/142/5/145.
20. W. De Blok, J. Van Der Hulst, and G. Bothun, Monthly Notices of the Royal Astronomical Society, **274**, 235 (1995).
21. Y. Rashed, J. Zuther, A. Eckart, G. Busch, M. Valencia-S, M. Vitale, S. Britzen, and T. Muxlow, Astronomy & Astrophysics, **558**, A5 (2013). https://doi.org/10.1051/0004-6361/201322211.
22. D. G. York, J. Adelman, J. E. Anderson, S. F. Anderson, J. Annis, N. A. Bahcall, J. Bakken, R. Barkhouser, S. Bastian, and E. Berman,The Astronomical Journal, **120**, 1579 (2000).
23. K. Accetta, C. Alert's, V. S. Aguirre, R. Ahumada, N. Ajgaonkar, N. F. Ak, S. Alam, C. A. Prieto, A. Almeida, and F. Anders, The Astrophysical Journal Supplement Series, **259**, 35 (2022). https://doi.org/10.3847/1538-4365/ac4414.
24. I. Martinez-Valpuesta, J. Knapen, and R. Buta, The Astronomical Journal, **134**, 1863 (2007).
25. E. Athanassoula, The Astrophysical Journal, **569**, L83 (2002).

26. A. K. Ahmed, Australian Journal of Basic and Applied Sciences, **11**, 1 (2017).
27. A. H. Abdullah and P. Kroupa, Astronomy letters, **47**, 170 (2021). https://doi.org/10.1134/S1063773721030014.
28. L. Y. A.-S. Mashhadani and A. H. Abdullah, NeuroQuantology, **18**, 18 (2020). https://doi.org/10.14704/NQ.2020.18.12.NQ20233.
29. A. Almeida, S. F. Anderson, M. Argudo-Fernández, C. Badenes, K. Barger, J. K. Barrera-Ballesteros, C. F. Bender, E. Benitez, F. Besser, and J. C. Bird, The Astrophysical Journal Supplement Series, **267**, 44 (2023). https://doi.org/10.3847/1538-4365/acda98.
30. E. Athanassoula, M. Romero-Gómez, A. Bosma, and J. Masdemont, Monthly Notices of the Royal Astronomical Society, **400**, 1706 (2009).https://doi.org/10.1111/j.1365-2966.2009.15583.x.
31. J. Sellwood, Reviews of Modern Physics, **86**, 1 (2014).
32. M. Schwarz, Monthly Notices of the Royal Astronomical Society, **209**, 93 (1984).
33. J. Kormendy, Astrophysical Journal, Part 1, **227**(1), 714 (1979).
34. M. Cappellari, Annual Review of Astronomy and Astrophysics, **54**, 597 (2016). https://doi.org/10.1146/annurev-astro-082214-122432.
35. J. C. Lee, H. S. Hwang and H. Chung, Monthly Notices of the Royal Astronomical Society, **477**, (2018). https://doi.org/10.1093/mnras/sty729.
36. D. G. Tolasa, Archives of Engineering and Technology, **2**, 1 (2025). https://www.doi.org/rpc/2025/rpc.aei/00235.
37. A V. Semenov, V. Tymchyshyn, V. Bezguba, M. Tsizh, and A. Khlevniuk, Astronomy and Computing, **52**, 100963, (2025). https://doi.org/10.1016/j.ascom.2025.100963.
38. K. C. Freeman, Astrophysical Journal, **160**, 811 (1970).
39. R. J. Buta, Astrophysical Journal, Part 1, **351**(1), 62 (1990).
40. G. G. Byrd, T. Freeman, and R. J. Buta, The Astronomical Journal, **131**, 1377 (2006).

التحقيق في البنية الحلقية المعقدة للمجرة NGC 10168: تحليل فوتومتري وبنيوي لمجرة مصنفة كـ (R₁R'₂)SABa(r'l)a

زينب فاضل حسين[1] وعبد الله كامل احمد[1]

[1] قسم الفلك والفضاء، كلية العلوم، جامعة بغداد، بغداد، العراق

الخلاصة

تقدم هذه الدراسة تحليلًا ضوئيًا وبنيويًا شاملًا للمجرة UGC 10168، المصنفة على النحو (R₁R₂′)SABa(r′l)a ضمن نظام CVRHS (Comprehensive de Vaucouleurs Revised Hubble-Sandage). تُعد UGC 10168 مجرة لولبية ذات قضيب من النوع المتوسط، تحتوي على هياكل حلقية داخلية وخارجية معقدة، مما يجعلها نموذجًا مثيرًا لدراسة ديناميكيات السمات الرنينية. نستخدم القياسات الضوئية السطحية لتحليل توزيع اللمعان، والاهليجية، وزاوية الموضع على طول المحور شبه الرئيسي للمجرة، وذلك بالاعتماد على صور متعددة الأطوال الموجية من مسح سلون الرقمي للسماء (SDSS). يشير التصنيف (R₁R₂′) إلى وجود حلقتين زائفتين خارجيتين مميزتين ناتجتين عن التفاف الأذرع الحلزونية، في حين يشير (r′l) إلى حلقة داخلية غير منتظمة تحيط بالقضيب. تساهم بنية القضيب (SAB) والخصائص الحلزونية المبكرة (Sa) في تشكيل بنية معقدة نقوم بتحليلها تفصيليًا باستخدام تقنيات التحليل الضوئي البنيوي . يُحتمل أن تكون الحلقتان R₁ و R₂′ مرتبطتين بديناميكيات القضيب وتأثيرات رنينLindblad، حيث تكشف نتائجنا عن سمات رنينية بارزة . تم تحليل توزيعات الألوان المحسوبة من فروقات الشدة بين مرشحات SDSS (g-r, r-i, و i-z) لدراسة التدرجات في التجمعات النجمية ومستويات تشكل النجوم ضمن الحلقات والقضيب والقرص. تُظهر الفروقات اللونية بين الحلقات الداخلية والخارجية اختلافات في أعمار النجوم ومناطق تشكل النجوم المتأثرة بالرنينات. تُعزز هذه الدراسة فهمَ نشوء الحلقات وأحداث الرنين في المجرات الحلزونية الضلعية، مُقدِّمةً رؤىً حول مسارات تطورها ضمن إطار ديناميكياتها وشكلها المجري.

الكلمات المفتاحية: المجرة، CVRHS، UGC 10168، SDSS، الحلقات الزائفة.